Multilevel optimization of a supersonic aircraft

M. Vázquez*, A. Dervieux† and B. Koobus‡

February 27, 2004

Keywords: Multilevel Optimization, Preconditioner, Adjoint Formulation, Transpiration Conditions, Sonic Boom Reduction

This paper investigates the application of a multilevel preconditioned algorithm for the sonic boom reduction of a supersonic business jet. The optimisation algorithm relies on a gradient approach with an adjoint state evaluation. The multi-level preconditioner is designed from an analysis of the gradient regularity loss. The sonic boom reduction is achieved in an indirect way by minimizing what we call the sonic boom downwards emission, which is computed in the near field. Additional aerodynamic performances like lift and drag forces are also guaranteed by including their evaluation in the problem's cost functional. Applications to 3D geometries are presented.

*INRIA, 2004 Route des Lucioles, BP. 93, 06902 Sophia-Antipolis, France

†INRIA, 2004 Route des Lucioles, BP. 93, 06902 Sophia-Antipolis, France

‡Université de Montpellier II, Dept Mathématiques, CC.051 34095 Montpellier Cedex 5, France

List of Figures

1 Introduction

In the last two decades, the progress made in the optimization domain has completely renewed the panoply of optimizers. When differentiable optimization is considered, Sequential Quadratic Programming (SQP) algorithms have replaced gradient ones, thanks to the integration of very efficient quasi-Newton strategies. These methods directly address the optimality conditions and, more frequently, handle parameters that are discrete representations of smooth functions. However, since the new optimization theory and methods are built in $\mathbb{R}^n$, the outcome of the process may loose its original smoothness.

To illustrate this, consider the "best-seller" problem of the calculus of variations:

$$\text{Find} \quad \bar{u} \quad \text{such that} \quad \bar{u} = \arg\min_u \quad \frac{1}{2}\int |\nabla u|^2 dx - \int u \ f \ dx \ , \tag{1}$$

choosing $\bar{u}$ within a given subspace. The functional to minimize represents the key concept in any optimization problem, where it is usually known as *cost functional*. It quantifies the corrections brought to the unknown under certain given conditions and it is defined according to our needs. In most quasi-Newton optimization methods, the basic brick for the corrections which are applied to the unknown is the gradient of the functional (for the problem so defined by Equation (1))

$$g \quad = \quad -\Delta u - f. \tag{2}$$

which tells us how the unknown must be modified in order to get closer to our minimization objective. This correction has the important disadvantage to be a function much less regular than the previous iterate u. Indeed, if u has continuous derivatives up to k-th order, it is true only up to $(k-2)$-th for g. Consequently, the iterative process of an algorithm relying on g, of the kind

$$u^{n+1} = u^n \ - \ \rho \ g, \tag{3}$$

would produce a new u with only $(k-2)$-th continuous derivatives, then $(k-4)$-th ones and so on. Ultimately, it will be impossible to compute the functional to minimize.

It is well known that, after discretization, using g for building corrections is equivalent to apply a Jacobi iteration. This will amplify many high frequency modes, unless the step length is reduced in order to satisfy a Courant-like stability condition. In this case, if the discretization is fine and the high frequency modes are very numerous, the quasi-Newton process cannot compensate the

difficulties in converging. This is why quasi-Newton solvers for Partial Differential Equations (PDE) are generally associated with preconditioners.

By the way, we note the strong relation between preconditioners and smoothers in this context. In the $\mathbb{R}^n$ theory, a preconditioner is used basically to improve the condition number of a linear system, that is to reduce the ratio between the largest and the smallest eigenvalue. In the discrete PDE case, ill-conditioning comes from mesh dependent high frequency eigenvalues, that increases with mesh fineness and with the degree of differential operator. Then two ways of reducing this effect is either to use a coarse mesh, not an acceptable solution, or to apply special devices for filtering high frequencies. In the functional context, it seems necessary (and somewhat equivalent to the above strategies) to work with an iterative correction in which regularity is not lost, for example by multiplying it by an inverse Laplace operator, so that the order of derivatives should be recovered.

Then the functional iteration can be done in a smooth manner, converging at its own convergence speed. An important consequence is that a good discretization of this iteration should ideally have a convergence rate close to the functional one, that is a mesh-size independent rate. Then, building a preconditioner that renders the functional iteration regularity will increase the potential qualities of the discretized iteration.

To sum up, the principle we shall follow is to introduce a preconditioner or smoother inspired by functional properties in order to improve the optimization iteration of our optimal shape design problem. More precisely, we shall apply a multi-level preconditioner studied in a companion paper [1] to the present one. This multi-level preconditioner is of Bramble-Pasciak-Xu type. Its particularity is that it applies to a large family of unstructured triangulations or tetrahedrizations. The key principle for its application is the identification of the loss of regularity and its compensation.

The application of this stategy assumes that we have a good knowledge of the global optimality system to solve, including the functional properties: in particular, continuous and discrete gradient do not appear here as competitors, but as complementary aspects of the problem. The continuous gradient derivation, in its typical form of a Hadamard formula, contributes to the understanding of the singularity arising in an optimum design gradient. Its analysis helps for the choice of the particular multi-level preconditioner that we will apply.

We shall illustrate these remarks on concrete shape optimal design problems in Aeronautics. The optimization of supersonic transports is one of today's

challenge in the field. We will concentrate in the optimization of the aerodynamic performances together with the sonic boom emission for supersonic aircrafts, following a method firstly proposed in [2].

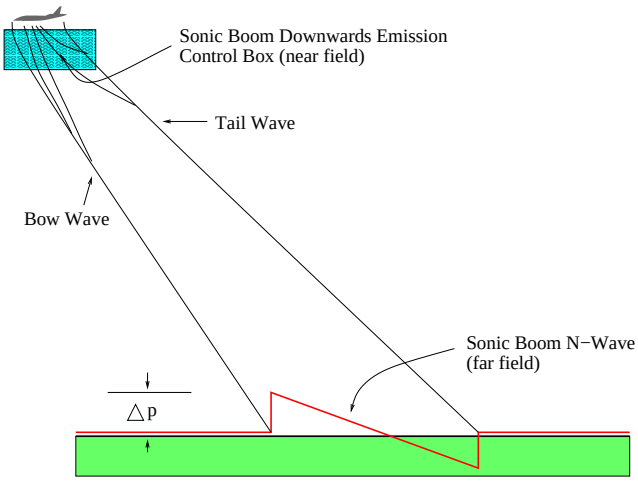

Figure 1: The sonic boom. Sketch of near and far field shock wave patterns of a supersonic aircraft.

Let us introduce the general idea. Any solid body moving at a supersonic speed developes a shock wave system. A simple solid of revolution (like a projectile) produces essentially only two shock waves, one in front and the other one behind. Although more complex bodies, like airplanes, produce more complex shock patterns which coalesce beyond the near field. Figure 1 sketches the situation. Once the shock waves pattern reaches the soil, it has ultimately become a two-shock system, which is called an N-type pressure wave, which is dragged by the plane movement. Both the initial pressure rise and final drop are steepened after propagation through the atmosphere, producing very strong explosive sounds on the ground, which for instance lays at 15 km below the airplane for the Concorde flying at cruise altitude. This fact has motivated the prohibition of Concorde supersonic flights over land. Therefore, the reduction of the sonic boom is an important issue in the specification of the next generation of supersonic aircrafts [3, 4]. According to [4], sonic boom minimization could be attained by considering basically three points: to get the minimum pressure impulse, which is defined as the integral of the absolute value of the overpressure ground signature, or the minimum initial shock pressure rise or finally to smooth the pressure rise by distributing it in a longer rise time. Different optimization strategies focus on one or several of these possibilities.

The remainder of this paper is organized as follows. The next section introduces the multilevel functional optimization problems in the context of

an adjoint formulation and proposes a solution to gradient's regularity loss, which is in turn studied with the aid of a Hadamard's formula for transpiration boundary conditions. Then, the sonic boom optimization is addressed in terms of what we call the sonic boom downwards emission, **(SBDE)**. Next, a serie of numerical studies validates the proposed solutions. Two particular aspects are analyzed: the regularity loss and the transpiration conditions for 3D problems. The section concludes with a numerical example. A projected supersonic business jet is optimized following the proposed scheme. This project is currently being developed at Dassault Aviation, which has kindly provided the mesh for this problem. Finally, in the last section we conclude this paper and give plans for future research.

2 Functional optimization

As announced in the introduction, gradients in optimal shape design need functional preconditioning. This can be done by applying an elliptic operator on shape perturbations, see for example [5] or [6]. We are here interested in a more sophisticated preconditioning. In a companion paper [1] to the present one, the building and the effect of a wavelet or a Bramble-Pasciak-Xu family of preconditioners is examined in the context of 3D shape design. The next subsection presents this family. Then we describe the optimal shape problem to solve and we identify which preconditioner of the above family should be applied.

2.1 Multilevel preconditioner

The shape of a volumic solid aircraft geometry can be discretized as a non-plane triangulated surface in 3D. Let Σ_0 be the initial 3D surface, made of triangles. The generic discrete surface Σ_γ is defined by the translation of length (also denoted) γ along an approximate unit normal vector $\vec{n}$ defined at the vertices of Σ_0. Therefore,

$$\vec{x}_i^\gamma \text{ is a vertex of } \Sigma_\gamma \quad \Leftrightarrow \quad \vec{x}_i^\gamma = \vec{x}_i^o + \gamma(i)\ \vec{n}_i \tag{4}$$

where i is the index of the vertex, $\vec{x}_i^o$ is the physical position of the vertex of Σ_0 with same index i.

Let g be a descent direction for γ. It is defined on the so-called fine level and allows to build a corrected shape: $\Sigma_{\gamma+\delta\gamma}$. We note that the coarse level is

an arbitrary unstructured mesh without any pre-built hierarchy. Let us first explain how a coarser level is defined. A coarser level is built by grouping together several fine nodes. Basis functions, that are unity-valued over each of these groups and zero otherwise, are not enough regular. Then we introduce a regular projection to a coarser level given by: $\mathcal{L}\mathcal{P}\mathcal{P}^*\mathcal{L}^*$, where $\mathcal{P}^*$ is the canonical projection to the coarser level, $\mathcal{P}$ (transpose of $\mathcal{P}^*$) denotes a prolongation to the initial level, and $\mathcal{L}$ is the smoothing operator defined as an averaging weighted by a scalar product of normals:

$$(\mathcal{L}\ \vec{x})_i = (1-\theta)\vec{x}_i + \theta\ \frac{\sum\limits_{j\in\mathcal{V}(i)\cup\{i\}} w_{ij}\vec{x}_j}{\sum\limits_{j\in\mathcal{V}(i)\cup\{i\}} w_{ij}} \tag{5}$$

where w_{ij} are the weights given by :

$$w_{ij} = \max\ (Area(i)\cdot Area(j)\cdot\vec{n}_i\cdot\vec{n}_j\ ,\ 0) \quad \|\vec{n}_i\| = 1\ \ \forall\ i, \tag{6}$$

being θ the smoothing parameter. $\mathcal{V}(i)$ represents the neighbors of cell i and $Area(i)$ is the measure of its area.

With the above transfer and smoothing operators from any level $m-1$ to level m as elementary bricks, we can derive a projection operator related to level k:

$$P_k \quad = \quad \prod_{1\leq m\leq k} \mathcal{L}_m\mathcal{P}_m\mathcal{P}_m^*\mathcal{L}_m^*. \tag{7}$$

This set of operators is used to construct the *Additive Multilevel Preconditioner* (**AMP**) as follows:

$$P^{\text{AMP}}g \quad = \quad P_n g \quad - \quad \sum_{k=1}^{n-1} \quad \left(\frac{1}{2^a}\right)^{n-k} \ (P_{k+1}g \ - \ P_k g) \tag{8}$$

where n is the coarsest level. The multiplying factor involves the characteristic element lengths ratio between two consecutive levels (2 in this case, by construction). It involves an exponent a, which is supposed to be the **differentiability degree lost by the gradient** g. This degree is the only information to get from the systems to solve, since the rest of the preconditioner derivation does not depend on the nature of the PDE and on the functional definition involved in the present problem. However the evaluation of this degree is of crucial impact on the quality of the preconditioner. In order to identify it, we need to analyse our particular optimization problem. This is carried out in the next two sections.

2.2 Problem statement - Adjoint formulation.

In order to evaluate the gradients that will drive the optimization process, the control theory provides an elegant and efficient method which by-passes the costly alternative of computing them with finite differences. The use of this method for aerodynamical design was introduced by Jameson in the classical reference [7]. Basically, it consists of a minimization problem under a particular additional constraint: the flow equations themselves.

The general form of the problem to solve is then the following: we want to find γ_0 that minimizes a certain functional $j(\gamma) = J(\gamma, W(\gamma))$ under the constraint $\Psi(\gamma, W(\gamma)) = 0$. All γ's represent the parametrization of the shape to optimize. $j(\gamma)$ is the cost functional mentioned above, whose dependence on γ is set by the aerodynamics community according to certain needs. Finally, the constraint $\Psi(\gamma, W(\gamma)) = 0$ is the set of flow equations, in this case the compressible Euler equations, solved in a domain Ω for which $\partial\Omega \supset \gamma$, being $W(\gamma)$ the flow field.

The minimization problem is then solved using Lagrange multipliers. The problem's Lagrangian is

$$L(W, \gamma, \Pi) \;=\; J(W, \gamma) + \langle \Psi(\gamma, W), \Pi \rangle, \tag{9}$$

where Π is a generalized Lagrange multiplier, and $\langle\ ,\ \rangle$ is a suitable scalar product. Then, γ_0 is found after solving

$$\begin{aligned} &\Psi(\gamma, W(\gamma)) = 0 \\ &(\nabla_W \Psi(\gamma, W(\gamma)))^* \;\; \Pi = \nabla_W J(\gamma, W(\gamma)) \\ &j'(\gamma) = \nabla_\gamma J(\gamma, W(\gamma)) \quad - \quad \langle \Pi(\gamma), \nabla_\gamma \Psi(\gamma, W(\gamma)) \rangle. \end{aligned} \tag{10}$$

The first line is the **flow solution**, to obtain $W(\gamma)$. The second one is the so called **adjoint flow solution**, to get $\Pi(\gamma)$. And in the last line, the **gradient** $j'(\gamma)$ of the cost functional is evaluated, which in turn will be used to modify the former γ. The derivatives of both the constraint and the cost functional can be obtained either by finite differences or, much more efficiently, by automatic/analytic differentiation [6].

The multilevel gradient approaches considered here rely on the algorithm in Table 1. Here, for each iteration nc, $g(\gamma, W, \Pi)$ is a function of variables γ, W and Π , that is identical to $j'(\gamma)$ only if $W = W(\gamma)$ (solution of the state equations) and $\Pi = \Pi(\gamma)$ (solution of the adjoint state equations). The parameter ρ is either fixed or defined by a 1D search (steepest version). If P^{AMP} is the identity, this algorithm results in a *gradient method* when g is

Multilevel Preconditioned Algorithm

Do nc

- Compute state W and adjoint Π
- Compute gradient $g(\gamma^{nc}, W, \Pi)$
- Compute the preconditioner P^{AMP}
- Compute ρ (internal cycle)
- Update the shape correction:

$$\gamma^{nc+1} \;=\; \gamma^{nc} - \rho \;\; P^{\text{AMP}} \; g(\gamma^{nc}, W, \Pi)$$

Next nc

Table 1: Multilevel Preconditioned Algorithm

exactly $j'(\gamma)$. In the preconditioned case, we get a descent direction in a weak sense since the preconditioner is symmetric positive.

It is worth to mention that if the state equations and the adjoint state equations are not completely solved, $g(\gamma, W, \Pi)$ is not the gradient of $j(\gamma)$. However, $g(\gamma, W, \Pi)$ tends towards $j'(\gamma)$ when the whole loop is converging; we refer to that algorithm as a **one-shot method** (according to [8]) for solving the optimality system of the optimization problem (see a discussion for 2D applications in [9]). In this paper we have not used that approach.

2.3 Hadamard's formula and regularity issues

The solution of a Poisson problem can be differentiated with respect to the variation of the geometrical domain boundary. This was first done by J. Hadamard. It was rigourously revisited within the functional context of Sobolev spaces for Poisson problems in [10]. In fact, this analysis cannot be optimal unless it is derived in Holder spaces. An optimal study proposed in [1] shows that first order variations are spatially less regular functions than the original Poisson solution. This loss of derivative is an obstacle to the fast convergence of a gradient method. The rigorous Hadamard differentiation with respect to the geometrical domain for the compressible Euler model is today out of reach. However, in several works and in particular in [11], [12], a *formal* Hadamard differentiation is proposed. The object of this section is to recall briefly the

conclusion of those studies, and then to adapt it to the case of transpiration conditions and to finally address it to the loss of derivative in the continuous context.

Let us consider an optimal shape design problem in which the domain Ω_γ of R^d is parametrized by a displacement γ of a part of the boundary in the normal direction V to an initial geometry Ω_0, as shown in Figure 2. In the other part of the boundary, we consider far field conditions that do not need to be precised further for our argument.

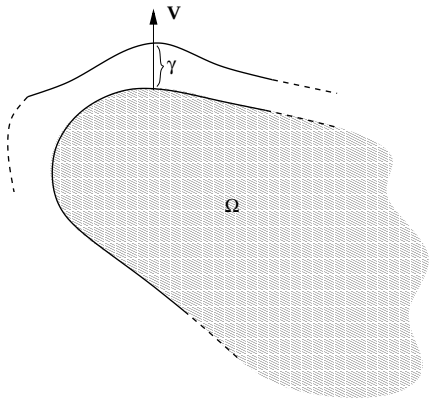

Figure 2: Boundary parametrization.

Let D be a subdomain of Ω_γ (inside Ω_γ for any admissible γ). We consider the minimization of the following functional:

$$j(\gamma) \;=\; \frac{1}{2}||W(\gamma) - W_{target}||^2_D \;.$$

The state equation is the set of steady Euler equations with appropriate boundary conditions. It is represented in a variational form as follows: for all $\phi = (\phi_1, \phi_2, \phi_3, \phi_4, \phi_5)$ belonging to the appropriate space,

$$\begin{aligned}(\Psi(\gamma, W), \phi) \;&=\; -\int_{\Omega_\gamma} (F(W)\frac{\partial \phi}{\partial x} + G(W)\frac{\partial \phi}{\partial y} + H(W)\frac{\partial \phi}{\partial z})\; d\Omega_\gamma \\ &+\; \int_{\partial\Omega_\gamma} p\;(n_x^\gamma\;\phi_2 \;+\; n_y^\gamma\;\phi_3 \;+\; n_z^\gamma\;\phi_4)\; d\partial\Omega_\gamma = 0, \qquad (11)\end{aligned}$$

where the Euler fluxes are $F(W), G(W)$ and $H(W)$, corresponding respectively to each of the space directions. The exterior normal $\vec{n}^\gamma$ to $\partial\Omega_\gamma$ has components $(n_x^\gamma, n_y^\gamma, n_z^\gamma)$.

Admitting that some differentiability assumptions are fulfilled, the Gâteaux-derivative of j at γ_0 in the direction $\delta\gamma$ can be obtained after some computa-

tions (see [11]):

$$\begin{aligned} j'(\gamma_0,\delta\gamma) &= -\int_{\partial\Omega_{\gamma_0}} (F(W)\frac{\partial\Pi}{\partial x}+G(W)\frac{\partial\Pi}{\partial y}+H(W)\frac{\partial\Pi}{\partial z})(\vec{n}^{\gamma_0}\cdot\vec{V})\ \delta\gamma d\partial\Omega_{\gamma_0} \\ &+ \int_{\partial\Omega_{\gamma_0}} (\nabla p\ \Pi\ +\ p\ \nabla\Pi)(\vec{n}^{\gamma_0}\cdot\vec{V})\ \delta\gamma d\partial\Omega_{\gamma_0} \end{aligned}$$

with the following notations,

$$\begin{aligned} \nabla p\ \Pi &= \frac{\partial p}{\partial x}\ \Pi_2\ +\ \frac{\partial p}{\partial y}\ \Pi_3\ +\ \frac{\partial p}{\partial z}\ \Pi_4, \\ p\ \nabla\Pi &= \frac{\partial \Pi_2}{\partial x}\ p\ +\ \frac{\partial \Pi_3}{\partial y}\ p\ +\ \frac{\partial \Pi_4}{\partial z}\ p. \end{aligned}$$

The adjoint state Π is solution of the system:

$$\left(\frac{\partial F}{\partial W}\right)^*\frac{\partial\Pi}{\partial x}+\left(\frac{\partial G}{\partial W}\right)^*\frac{\partial\Pi}{\partial y}+\left(\frac{\partial H}{\partial W}\right)^*\frac{\partial\Pi}{\partial z} = -(W(\gamma_0)-W_{target})\chi_{\rm D} \quad \text{on} \quad \Omega_{\gamma_0},$$

where $\chi_{\rm D}$ is the characteristic function of D and with boundary condition:

$$\Pi_2 n_x^{\gamma_0}+\Pi_3 n_y^{\gamma_0}+\Pi_4 n_z^{\gamma_0} = 0 \quad \text{on} \quad \partial\Omega_{\gamma_0}.$$

Taking the L^2 space as pivot space for our gradient method would produce the following direction of correction for the boundary parameter γ:

$$\gamma = \gamma_o\ -\ \rho g_{L^2}(\gamma_o, W, \Pi)$$

where:

$$\begin{aligned} g_{L^2}(\gamma_o,W,\Pi) = &- (F(W)\frac{\partial\Pi}{\partial x}+G(W)\frac{\partial\Pi}{\partial y}+H(W)\frac{\partial\Pi}{\partial z})\ (\vec{n}^{\gamma_0}\cdot\vec{V}) \\ &+ (\nabla p\ \Pi\ +\ p\ \nabla\Pi)\ (\vec{n}^{\gamma_0}\cdot\vec{V})\ . \end{aligned} \tag{12}$$

We observe that this correction is generally much less regular than the boundary parameter γ_0. Indeed, inspired by elliptic smoothness, we can estimate that the state variables are at most as regular as the boundary, but the above correction involves derivatives of the adjoint state. Additionally, the normal vector $\vec{n}^{\gamma_0}$ is a derivative of the boundary. Regularity can be lost further if we try to cast this gradient iteration in a Hilbert context in order to enjoy a convergence theorem for the optimization iteration.

Let us now adapt this analysis to the case where the variable domain effect is approximated by the combination of a constant domain with a **transpiration condition**. We briefly recall the transpiration condition for Euler flows.

The slip boundary term of the flux $\Psi(W)$ is defined on a **fixed reference geometry** Ω_0 as follows: for each component of the Euler flow equations set (n^0 is the normal exterior to Ω_0),

$$\Psi(W)_{slip\ boundary} = q(\gamma)W + \Big(0\,,\, p(W)n_x^0\,,\, p(W)n_y^0\,,\, p(W)n_z^0\,,\, p(W)q(\gamma)\Big) \quad (13)$$

where

$$q(\gamma) = \vec{u}\ .\ (\vec{n}^0 - \vec{n}^\gamma)$$

in which $\vec{u}$ is the velocity of the fluid. The state equation writes in a form that is much similar to the above Euler model, i.e. for all ϕ we have

$$\begin{aligned}(\Psi_{\rm TP}(\gamma,W),\phi) &= -\int_{\Omega_0}(F(W)\frac{\partial\phi}{\partial x}+G(W)\frac{\partial\phi}{\partial y}+H(W)\frac{\partial\phi}{\partial z})\ d\Omega_0\\ &+ \int_{\partial\Omega_0} p\ (n_x^0\ \phi_2\ +\ n_y^0\ \phi_3\ +\ n_z^0\ \phi_4)\ d\partial\Omega_0\\ &+ \int_{\partial\Omega_0} q(\gamma)(W_1\phi_1+W_2\phi_2+W_3\phi_3+W_4\phi_4+(W_5+p)\phi_5)\ d\partial\Omega_0\\ &= 0, \end{aligned} \quad (14)$$

The label "TP" refers to the Euler flow with transpiration conditions. The derivation of the gradient is not so different from the previous one, so we do not give the details. The adjoint system at $(\gamma_0, W(\gamma_0))$ writes:

$$\left(\frac{\partial F}{\partial W}\right)^*\frac{\partial\Pi}{\partial x}+\left(\frac{\partial G}{\partial W}\right)^*\frac{\partial\Pi}{\partial y}+\left(\frac{\partial H}{\partial W}\right)^*\frac{\partial\Pi}{\partial z}=-(W(\gamma_0)-W_{target})\chi_{\rm D}\ \ \text{on}\ \ \Omega_0,$$

but now the boundary conditions write,

$$\begin{aligned}(\Pi_2 n_x^0+\Pi_3 n_y^0 &+ \Pi_4 n_z^0+q\Pi_5)\frac{\partial p}{\partial W_i}\\ &+ q\Pi_i+\frac{\partial q}{\partial W_i}\left(\Pi_i\sum_k W_k\ +\Pi_5 p\right)=0\ \forall i \text{ on } \partial\Omega_0\end{aligned}$$

The functional Gâteaux derivative turns to be:

$$j'_{\rm TP}(\gamma_0,\delta\gamma) = \int_{\partial\Omega_0}\left(\sum_k \Pi_k W_k\ +\Pi_5 p\right)\frac{\partial q}{\partial\gamma}\delta\gamma\ d\partial\Omega_0$$

We observe that the term q is a function of the normal vector n^γ. Now, in 2D case, the value $n^\gamma(s)$ at any curvilinear abscissa s of $\partial\Omega_0$ is a function f of $\gamma(s)$ and of the curvilinear spatial derivative $\gamma'(s) = \frac{\partial\gamma}{\partial s}(s)$ of γ. This writes as follows

$$n^\gamma(s) = f(\gamma(s),\gamma'(s)) \quad (15)$$

then

$$\frac{\partial n^{\gamma}(s)}{\partial(\gamma(s),\gamma'(s))}\delta(\gamma(s),\gamma'(s)) \quad = \quad \frac{\partial f}{\partial\gamma(s)}\delta\gamma(s)+\frac{\partial f}{\partial\gamma'(s)}\delta\gamma'(s) \tag{16}$$

but this can be also expressed from the Gâteaux derivative of n^{γ} with respect to γ:

$$(\frac{\partial n^{\gamma}}{\partial\gamma}\delta\gamma)(s) \quad = \quad \frac{\partial f}{\partial\gamma(s)}\delta\gamma(s)+\frac{\partial f}{\partial\gamma'(s)}\delta\gamma'(s) \tag{17}$$

and thus:

$$\frac{\partial q}{\partial\gamma}\delta\gamma \quad = \quad -\ u\ \left(\frac{\partial f}{\partial\gamma}\delta\gamma+\frac{\partial f}{\partial\gamma'}\delta\gamma'\right)\ . \tag{18}$$

Then we still get an expression involving first-order derivatives of the shape variables, as in (12). The 3D case is analogous.

These two examples show that in complex optimization problems, the direct application in R^N of gradient method, which is equivalent to choosing systematically the L^2 pivot space for the gradient iteration, may result in non-regular functional iterations. Further, it appears that the **loss in differentiability is formally 1**. If no preconditioner were introduced in order to compensate this loss of smoothness, the convergence would show a behavior analog to that of Jacobi or unpreconditioned Jacobi-type elliptic solvers, that is a very slow and mesh-dependent convergence.

3 Sonic boom optimization

In this section we apply the concepts introduced above in order to solve an optimal shape design application problem, namely the sonic boom optimization of an aircraft. The key point in sonic boom reduction is the same as in most of the optimization problems: it has to be attained without a prohibitive degradation of other flight qualities, in this particular case, related to the aircraft aerodynamical performance. Furthermore, a direct evaluation of the shock signature on the soil from the 3D Euler equations is nowadays computationally out of reach. It is necessary to model the far field sonic boom propagation, an issue described both in [3] through the pioneering works of Witham about the matter, and in [4]. The central idea in Witham's theory is to propagate bi-dimensionally, in a vertical plane spanned by the flight direction, the near field shock wave pattern, assuming some (indeed strong) hypotheses. This makes the pressure soil signature evaluation a problem separated from the

CFD simulation: it is a combination of a linearized propagation theory for the far field signature and a non linear three dimensional set of equations (Euler's or Navier-Stokes') for the near field flow.

We have identified two recent leading works on sonic boom optimization which follow this line, within the gradient methods context. One alternative is presented in [13]. In this work, it is proposed a parametrical optimization scheme for the sonic boom, where the spatial parameters are determined by several position coordinates of flying appendages (like canards) and nose tilting. The signature is modelled by the linearized theory as a function of some geometric aircraft parameters. In the reduced design parameters' space, an adjoint flow problem is solved in order to compute the cost functional gradient. Then the problem results in a minimization of only the initial shock pressure rise (ISPR), **leaving aside any reduction of the rest of the signature features**. The other alternative is to increase the parameters space by taking a finer parametrization of the *shape* itself of the wings and/or appendages: in [14, 15] an adjoint method is again used to optimize a model supersonic aircraft by modifying the positions of the discretized skin mesh (in [6], this kind of shape parametrization is christened **"CAD-free"**, conversely to the **"CAD-based"** parametrization like that of [13], which uses a reduced parameters space. We will follow this nomenclature too). In this case also, the far field pressure is computed, but now as a function of the near field pressure and as a result of an inverse problem **given a target pressure ground signature**. This is done by solving two coupled adjoint problems. Another novel "CAD-free" approach is that of [16], where the sonic boom is reduced in an indirect way by considering a special drag function in the objective. The pressure ground signature is evaluated by using a waveform parameter method. The optimization procedure is carried out using a combination of reduced complexity models for the far field depending sensitivity and incomplete sensitivities for the aerodynamical performance.

Although using a totally different method, it is worth to mention [17], as cited in both [14] and [13], where instead of solving the adjoint problem, these researchers use a genetic algorithm approach.

We propose a different, yet simplified way of sonic boom optimization. Assuming that the source of the pressure signature on the soil is the near field shock pattern below the airplane (we call it the **sonic boom downwards emission**, SBDE), by reducing it, the pressure signature will be consequently reduced. This fact is clearly seen in the previously cited references [16, 14]. In this way, after attaining a near field SBDE's reduction, the far field could be evaluated, but out of the optimization cycle, just to check the results. We propose, as a first approach, to quantify the SBDE as the pressure gradient

squared norm **integrated in a given "control box"** below the airplane and neighboring it, which is in fact a part of the CFD domain. The cost functional includes also terms related to flight performance (lift and drag). Constructive features, like wing thickness, can be treated by the sort of gradient projection introduced above.

The main differences relative to the alternatives referenced above are related to the sonic boom quantification. While in [14, 15], a target far field pressure distribution is given, in [13], the goal is to minimize only the ISPR. In the former case, the optimization is done over the shape of the complete aircraft and in the latter in a reduced design parameters space. In both cases, there is a sort of additional constraint in the minimization problem, imposed by limiting the space of solutions: either giving a target pressure or focusing only in the ISPR. We believe that depending on what is the requested goal, this approach can be sometimes very convenient. However, our analysis is free of this constraint, because we seek to minimize the near field SBDE, on the conviction that new aerodynamical shapes can be found, arising from the proposed minimization problem and retaining good flight performance. Our method is then complementary to other kinds of approach, like those described above. Another important difference is that all the works previously mentioned attack directly the full aircraft problem. In [2] we have already pointed out that optimizing very simple tridimensional forms using this method can give a deeper insight of the problem, about what is really producing the sonic boom. We propose then to start by optimizing *isolated* parts of the plane, as a preliminary step to the final stage, namely the full optimization of the plane.

3.1 Global approach. Transpiration conditions

We address now the transpiration boundary conditions, a key tool in our approach, its reliability being evaluated in the Numerical Examples section below. The numerical method used for predicting the steady Euler flows is a finite volume scheme. The numerical flux evaluation is done following Van Leer flux vector splitting, a choice depending on factors like robustness or problem size. The overall differentiability of the process will allow to apply an exact-gradient approach. The application of a shape design loop should involve the repeated rezoning of the mesh to take into account the modifications of the aircraft's shape. In this work, inspired by the approach used by Young *et al.* [18], we consider in a first phase the option of representing the shape modification by applying a transpiration condition; this means that the current shape is defined with respect to the mesh skin as a perturbation simulated by transpiration (see for example [19]), referred in the sequel as the "*transpired perturbation*". Then

γ is the perturbation function; it is the algebraic length of the displacement of the boundary along its normal.

The sensitivity analysis has been exactly derived. The validation of this sensitivity is performed by a direct comparison with divided differences of the cost function; the relative error in gradient components is about .001.

The global scheme is essentially made of three loops. The external loop is a remeshing loop in which a new shape is derived from an old one updated by the transpired perturbation. In the examples presented here, as the grid movements were not so important, this remeshing step is skipped. However, such a procedure was used to assess the correctness of the transpiration results (see Section 4.2). The extensive use of the outer remeshing loop is discussed in a forthcoming paper, where aeroelastic coupling is addressed and remeshing becomes necessary.

The medium loop is a gradient optimization one in which the control variable is the transpired perturbation; this loop involves the evaluation of the gradient of the cost functional through an adjoint state (see Table 1). We have discussed in previous works (e.g. [20]) the ability of the multilevel to converge with a speed that is rather insensitive to the number of parameters; we now stress that, although easily obtained by the multilevel method, the optimal control can still show spurious high frequencies. We found that their origin lied in the fact that normal vectors at nodes are not enough regular near very curved part of the surface geometry. Our answer to this problem is to smooth the normals defined at each node of the geometry.

Finally, the most internal loop is the 1D search in order to compute the steepest descent parameter ρ_{opt}.

3.2 Sonic boom downwards emission optimization

We propose here to measure the SBDE evaluating the volume integral of the squared pressure gradient in a control "box" (as shown in Figure 1) below the object. This is integrated in the cost functional as follows:

$$j(\gamma) = \alpha_1 (C_D - C_D^{target})^2 + \alpha_2 (C_L - C_L^{target})^2 + \alpha_3 \int_{\Omega^B} \frac{\partial p}{\partial x_i} \frac{\partial p}{\partial x_i} \; dV \qquad (19)$$

where α_1, α_2 and α_3 are constants that allow to prescribe the weights of the three constraints in $j(\gamma)$ that we want to consider, which are related to the aerodynamical performance (drag and lift) and the sonic boom emission.

Summation on repeated indices is assumed in the last term. From a practical point of view, the integration volume Ω^B is the part of the computational domain placed below the airplane, limited in its upper boundary by a plane below the aircraft and relatively close to it. It is worth to mention that the proposed method shows no particular dependence on the precise location of the upper limit of the SBDE's control box.

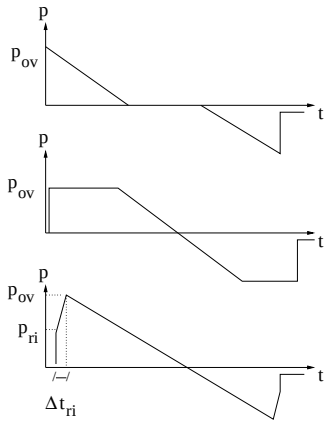

Figure 3: Overpressure ground signatures considered. Top, minimum impulse with overpressure peak p_{ov} (ISPR). Medium, minimum ISPR p_{ov}. Bottom, minimum ISPR p_{ri}, followed by a finite rise time Δt_{ri}, up to p_{ov}.

The question is basically the following: can a reduction in the volume integral that we call the SBDE be translated in a reduction in the ground shock signature? While, by using our method, we succeed in reducing the pressure peak *in the near field*, it could be asked what are the effects of this in the *far field*. A positive answer can be deduced from works where the near field (directly computed from the Euler equations) and the far field signature (computed in an *approximated* way as the far trace of the near field) are directly compared [15, 16, 14]. Additionally, in [2] we have given some hints to understand the effect, at least from a qualitative point of view, by analyzing 2D forms.

According to [4], there are three optimization goals related to ground pressure signatures, shown in Figure 3: the impulse, the ISPR and the finite rise time. The impulse is defined as the integral of the module of the pressure signature, the ISPR (initial shock pressure rise) and the rise time is the time for the pressure to rise up to its maximum value. While strong impulse values can produce important structural damage in the buildings affected, high ISPR and negligeable rise time have strong impact on creatures, and in particular, possible psychological consequences on human beings. We have observed (viz.[2]) that the shapes obtained by diminishing the SBDE with the proposed method, in general act on the combined effects, namely, reducing *all of the three* param-

eters, but on the *near* field. That is to say, the optimization process driven by the minimization of our cost functional *indirectly* acts on the cited parameters. It reduces both the ISPR and the impulse and it slightly increments the rise time. This can be seen in Figure 4, that shows the kind of results we have obtained. It shows the pressure distribution along a line below the midspan of an ONERA M6 wing for an Euler flow with a Mach number of 1.8 and an angle of attack of 3.0°. First of all, we have optimized the M6 wing. Then, we have created a 2D profile by cutting vertically through the 3D wing. Finally we have generated a partially refined 2D mesh to study the pressure pattern below the wing going up to several chord lengths. We acknowledge that this is a qualitative analysis. However, we believe that it goes in the proper direction. Further studies on the shockwave downwards propagation are currently carried on.

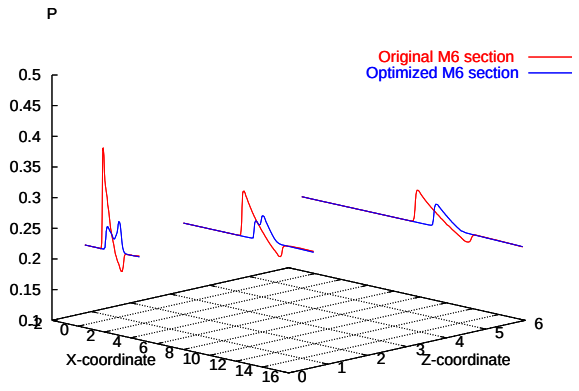

Figure 4: ONERA M6, 2D section of an optimized 3D wing. Pressure shock propagation below the airfoils at three different vertical positions placed at 0.5 , 3 and 6 chord lengths (this is the Z-coordinate).

4 Numerical Examples

4.1 The regularity loss

We have seen in Section 2 that the optimal exponent a in our preconditioner (see Equation (8)'s multiplying factor) should be taken larger or equal to the regularity loss. We have seen in Section 3 that this loss of derivation is at least 1. The purpose of this section is to try to observe by numerical experiments how the best measured exponent a_{opt} compares with the value predicted by theory. The idea is to check the efficiency of the proposed AMP applied to

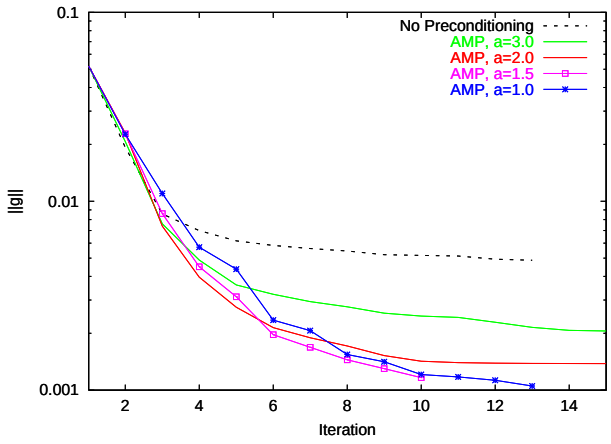

Figure 5: ONERA M6. Convergence rates for different values of the exponent a in the AMP definition equation (8).

an optimal design problem by evaluating its twofold claimed qualities: the regularity recovery and its smoothing properties. These virtues should both improve the convergence rate of the optimization procedure and produce better smooth shapes.

We have optimized a simple wing geometry. This geometry is an ONERA M6 wing, for incidence angle 3° and inflow Mach number 1.8. This optimization example is deeply studied in [2]. We have explored the values $a = 0$, 1 , 1.5 , 2 , 3, being $a = 0$ the equivalent to "No preconditioning". Figure 5 shows the convergence rates for the different values as the optimization iterative process advances. The gradient norm convergence (left) is clearly improved when the AMP is used, particularly with $1 \leq a \leq 2$. Convergence seem best for $a = 1$, but convergence is not much degraded for $a = 2$ and iterated shapes are smoother. Figure 6 illustrates this fact. It is a plot of the gradient norm along the downwards facing half wing taken along the mid-span, comparing again the different choices of a, including $a = 0$. The smoothing properties of the preconditioner is clearly seen. Consequently, the rest of the numerical experiments of this paper will be performed with the multilevel exponent equal to 2. The final asymptotic behavior of the gradient is due to the skin modifications which are restricted at the symmetry boundary.

4.2 Transpiration condition validation

In order to validate the 3D transpiration condition, we have carried out some numerical tests. The idea is to compute some flow parameters and to com-

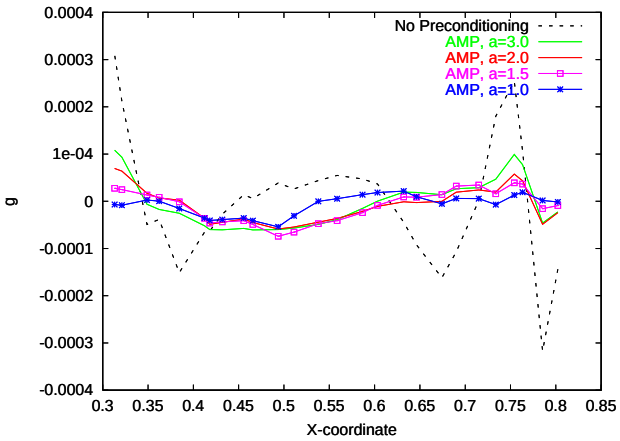

Figure 6: ONERA M6. Cost functional gradient. Distribution along the midline of the downwards wing surface after the first optimization iteration. Different values of the exponent a are compared.

pare them with and without transpiration condition. We have proceeded as follows. A single optimization iteration produces a modified shape. As stated above, the space of shape modifications is represented by a skin perturbation γ that runs along the normals at each skin node, according to the transpiration boundary condition. The original volume mesh can then be modified by adapting it to the "transpired" skin, producing a new mesh with the same number of nodes and elements. In our case, the new position of the interior grid points is determined from the displacement solution of a discrete pseudo-structural problem representing the unstructured dynamic mesh. The pseudo-structural system is constructed by lumping fictitious mass at each vertex of the mesh and attaching fictitious lineal springs at each edge connecting two vertices as well as fictitious torsional springs to each vertex [21]. The flow can then be recalculated with the new volume mesh and compared with that of the transpired conditions.

Table 2 shows the test results. Cost functional $j(\gamma)$ and lift and drag coefficients C_L and C_D computed for the original initial geometry are taken as a unitary reference. In this case, again the ONERA M6 is the chosen problem. The incidence angle is 3° and the inflow Mach number is 1.8. After a single optimization iteration, both $j(\gamma)$ and C_D has diminished and C_L remains approximately constant. In Table 2, the values between brackets represent the difference between those obtained with transpiration conditions accounting for the skin modifications and those of the corresponding remeshed volume. It is observed a relatively good accordance.

The remeshing algorithm can be used as a fine tuning correction for the

final optimized form. Once the iterative optimization process is finished, a new volume mesh can be generated to restart the problem. In this way, the normal skin vectors defined at each of the surface nodes will change according to the new discretization and, consequently, a new transpiration basis is obtained. This basis will be, supposedly, better adapted to the optimized surface. Additionally, the sensitivity to further shape modifications can be more accurately computed, although these modifications should be minor ones, in view of Table 2.

	$j(\gamma)$	C_L	C_D
Original (it=0)	1.000	1.000	1.000
Transpiration (it=1)	0.520	0.998	0.617
Remeshing (from it=1)	0.553 (+6%)	1.040 (+4%)	0.674 (+8%)

Table 2: Transpiration condition validation. Values relative to those evaluated in the original initial geometry. Between brackets, difference between transpiration and remeshing values.

4.3 Supersonic Business Jet

The example we show here is an optimum design study done on a projected Supersonic Business Jet, under developement at Dassault Aviation. It is also shown in [2], together with some other examples. The aircraft's geometry was provided by the constructor, as a spatial grid with 173526 nodes and 981822 tetrahedra, which corresponds to half of the aircraft and a vertical symmetry plane (see Figure 7). The inflow Mach number is 1.8 and the angle of attack is 3°.

The aircraft wings are the targets of the optimization. The simplified wings provided by the constructor for this generic geometry are horizontally symmetrical, with two different sweep angles of 17° and 38° respectively, and a rather smooth transition between them. The Mach angle for $M = 1.8$ is around 34°. Therefore, while the inboard part of the wings falls within the Mach cone (viz. [22]), producing a lower wave drag, the outboard wing cuts

through the Mach cone. As a consequence, the sharpest pressure gradients will be produced ahead of the *outboard* portion of the wing.

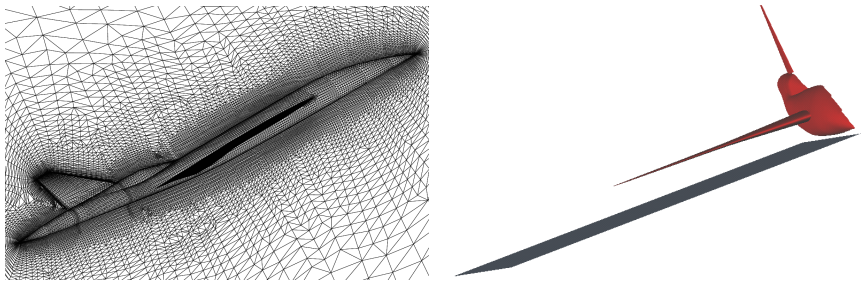

Figure 7: Dassault's Supersonic Business Jet. Right, spatial grid close-up. Left, aircraft and reference plane below.

This study is carried out in two steps, described in the next sub sections. Firstly, the aircraft wings are extracted from the plane, re-meshed with a coarser skin mesh, and optimized. In this way, the wings are totally isolated of the influence of the rest of the fuselage. This simplified geometry is used to do a preliminary study of the problem in which we show the effect of the three constitutive terms of the cost functional. Secondly, we optimize the wings, but now integrated in the original geometry of the aircraft, in order to see the influence of the fuselage in the wings optimization process. Figure 15 is clear: it shows the cost functional gradient distribution for the complete aircraft's surface at the initial optimization step. It tells which parts of the skin of the complete aircraft should be modified related to the sonic boom emission reduction. Combined with the isolated wings study, this could become a useful tool for aircraft designers.

4.3.1 Isolated wings: wing optimization

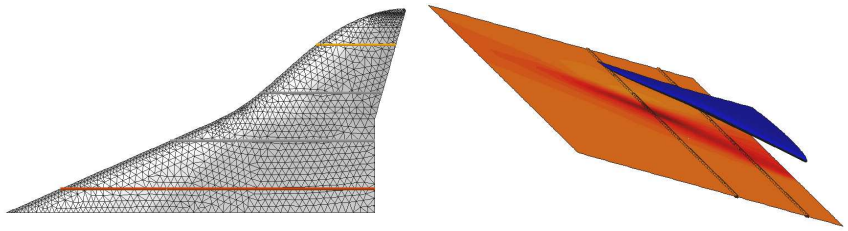

Figure 8: Isolated wings of the Supersonic Business Jet. Right, wing skin mesh and its four sections considered (the thick horizontal lines), named sections A, B, C and D from outside going inside towards the fuselage. Left, wing and reference plane below.

The skin mesh is shown in Figure 8 as well as the four cuts that are used in Figure 10 and which represents the physical stations where the effect of the optimization process is analyzed. The rather coarse skin mesh comprises 2409 nodes. In the same figure, at the bottom, it can be seen the wing and the plane below, which is at the top of the control box. The pressure distribution on this plane is used in Figure 9 to check how effective the sonic boom emission reduction is. We have followed two different optimization strategies in order to see the influence of the sonic boom reduction related to the lift and drag cost functional terms, using two different sets of parameters α, shown in Table 3 and named optimization strategies I and II. We have taken as target coefficients that of the original initial shape for the lift, and zero for the drag. Table 3 shows the values relative to the target ones.

In both cases, we seek to keep the drag and lift targets while reducing the sonic boom emission. The difference lays in the relative weight we assign to each of the terms in the cost functional. While the first strategy (I) enforces the aerodynamic performances, the second one is more aggressive for reducing the sonic boom emission (II). For both cases we also show the pressure distribution in the reference plane below, the wing profile at the four reference sections and the pressure distribution along a line below them.

	α_1 (in C_D term)	α_2 (in C_L term)	α_3 (in $\lvert\nabla p\rvert^2$ term)
Optimization Strategy I	1.0	10.0	0.001
Optimization Strategy II	1.0	10.0	0.1

Table 3: Isolated wings of the Supersonic Business Jet. Optimization strategies shown (α's coefficients are those used in the cost functional definition).

The pressure distribution below the wing after optimization clearly shows the two zones inside and outside the Mach cone, and the differences of both optimization strategies. In the outboard region, the shock is reduced, its top flattened and the rear over-expansion is almost eliminated, as seen in Figure 10. Although the strategy II seems to be more effective in the pressure peak reduction, both of them eliminate the over-expansion equally well. The strategy I produces a more uniform pressure distribution (see Figure 9), particularly in the inboard wing (see Figure 10, sections C and D). As described in [2],

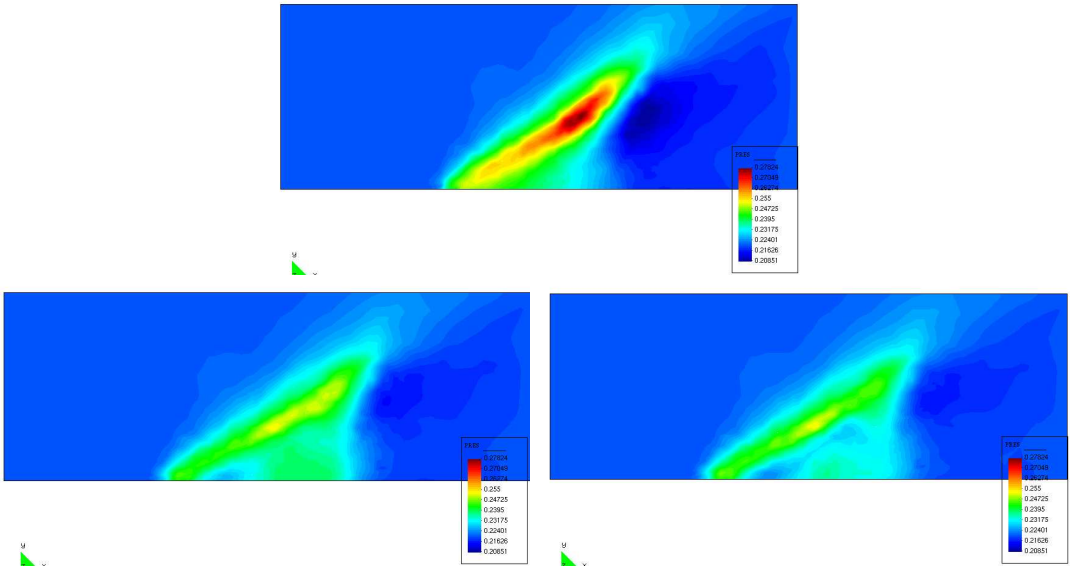

Figure 9: Isolated wings of the Supersonic Business Jet. Pressure distribution in the reference plane below the wing. Top, original geometry. Bottom, optimized geometries following strategies (I), left, and (II), right.

this study renders totally new wing shapes that are non-uniformly modified along the wingspan direction by the optimization cycle, as seen in the airfoils obtained in sections A, B, C and D, in Figure 11.

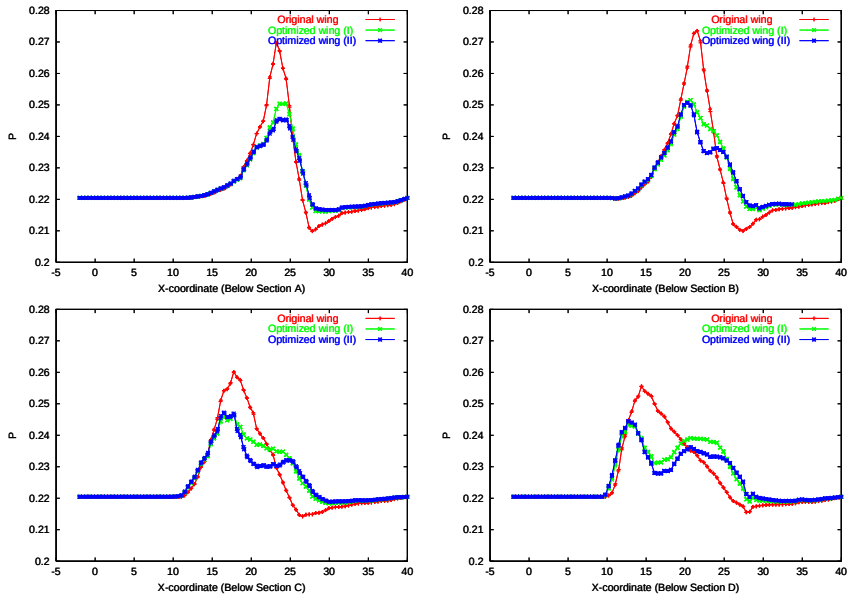

Figure 10: Isolated wings of the Supersonic Business Jet. Pressure along the lines projected by sections on the reference plane below the aircraft.

Figure 11 shows the original and the optimized airfoils obtained when cutting the wings in the four sections of Figure 8. Both optimization strategies include a by-sections volume preserving gradient projection technique (proposed in [2]). In order to prevent outboard-to-inboard mass migration, the volume preserving gradient is evaluated by dividing the wing-span in 30 sections and keeping the volume constant within each of them. For both strategies I and II, outboard and inboard optimized airfoils show a very different effect. As into the Mach cone the pressure gradients are much smoother, the two inboard airfoils do not develop an acute leading edge. Although their downwards sides are flattened, the leading edge remains blunt. On the other hand, the outboard optimized airfoils present very acute leading edges, particularly for the farthest outboard one. The strategy II tends to create more flattened outboard wing sections and more cambered inboard ones, due to its more aggressive effect on pressure peak reduction. Because of the volume preservation, this is translated in an outspread of the upper wing side, particularly in its rear part. On the other hand, the shape produced by the strategy I is smoother, because as the flattening and cambering of the downwards wing side is less, the upper side is also more uniform. This effect is in turn seen as a pressure overall flattening in the reference plane below the aircraft (see Figure 9). It is remarkable that for both strategies I and II, the inboard optimized shapes present the same tendency as that of [23], where only drag and lift are included in the optimization cost.

The most important difference in the results produced by the strategies I and II is not seen in the sonic boom downwards emission, which is reduced almost equally well in both cases, but in the aerodynamical wing properties, as shown in Table 4. The optimization strategy I leaves the aerodynamical performances almost intact. We recall that the aerodynamical coefficients targets are reached here only by wing cambering: we have left aside the incidence angle as a design variable for a next step in our research programme.

4.3.2 Integrated airplane: wing optimization

We continue this study with the complete airplane, of which Figure 12 shows the Mach number and pressure distribution over its surface (postprocessed using the symmetry plane as a "mirror"). Now, again only the wings are optimized but the influence of the rest of the plane is taken into account: it is deduced from these results that it is not at all negligeable.

The outcome of 8 iterations of the optimization strategy I is shown in Figure 13. In this figure it can be seen that the main peak has indeed diminished,

	C_L	C_L/C_D
Original	1.000	5.18
Optimization Strategy I	**0.982** (target 1.000)	**5.09**
Optimization Strategy II	0.895 (target 1.000)	4.25

Table 4: Isolated wings of the Supersonic Business Jet. Optimization strategies shown.

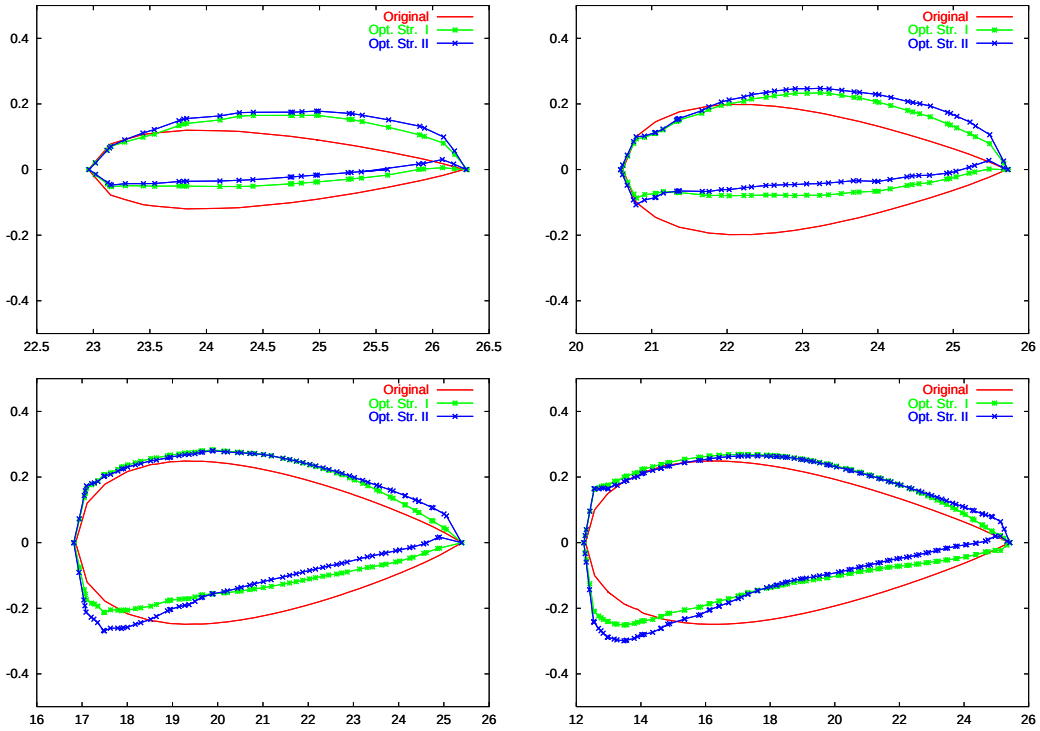

Figure 11: Isolated wings of the Supersonic Business Jet. Shape optimization shown at the four wing sections for both of the optimization strategies. Top: outboard sections A (left) and B. Right: inboard sections C (left) and D.

as in all the other cases. As for the optimization of the isolated wings, the optimization procedure has managed to damp the shock produced by the part

of the wing which is outside the Mach cone (Figure 14, left). However, within the Mach cone, the pressure peak has increased after the optimization process (Figure 14). This increase is slight, its maximum remains indeed close to that of the reduced shock. We believe that this fact can be attributed to the effect of the rest of the aircraft, especially the neighboring fuselage. As seen in Figure 15, the cost functional gradient distribution for the complete aircraft's surface tells us which parts of the skin of the complete aircraft should be optimized relatively to the cost functional proposed here. As a consequence of the application of our optimization procedure to this example, we can say that the optimization of the isolated aircraft parts could give deeper ideas to the designer about what really makes better shapes, even for rather coarse skin meshes. This optimization can be done much faster than that of the full aircraft and several different forms can be produced and tested until some of them are selected. This changes can be introduced in the full aircraft, and ultimately optimized completely to assess the changes.

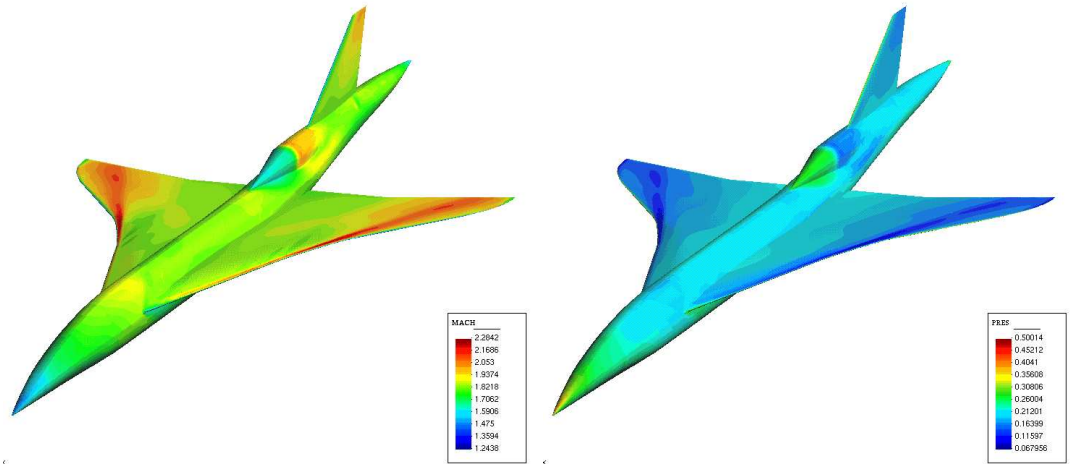

Figure 12: Supersonic Business Jet. Contour levels. Left, Mach number. Right, pressure.

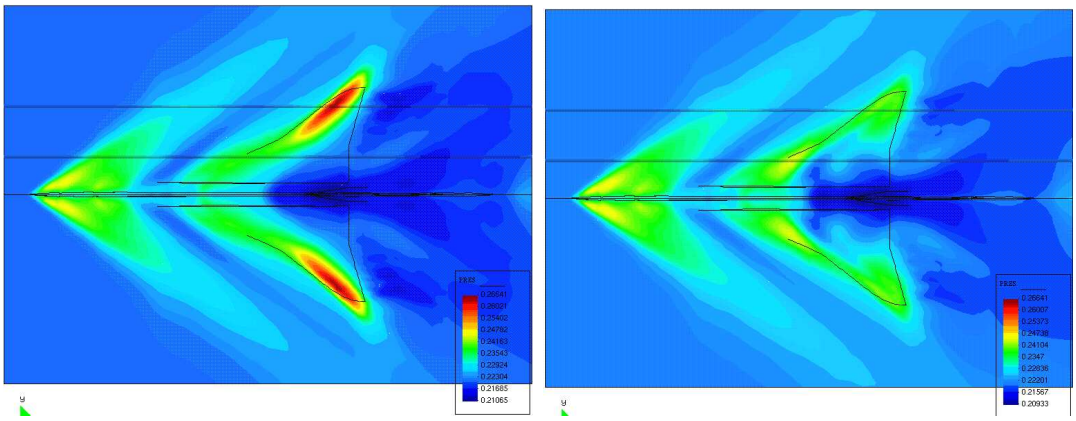

Figure 13: Supersonic Business Jet. Pressure distribution in a plane below the aircraft. Left, original geometry. Right, optimized geometry. The two lines of Figure 14 are shown here.

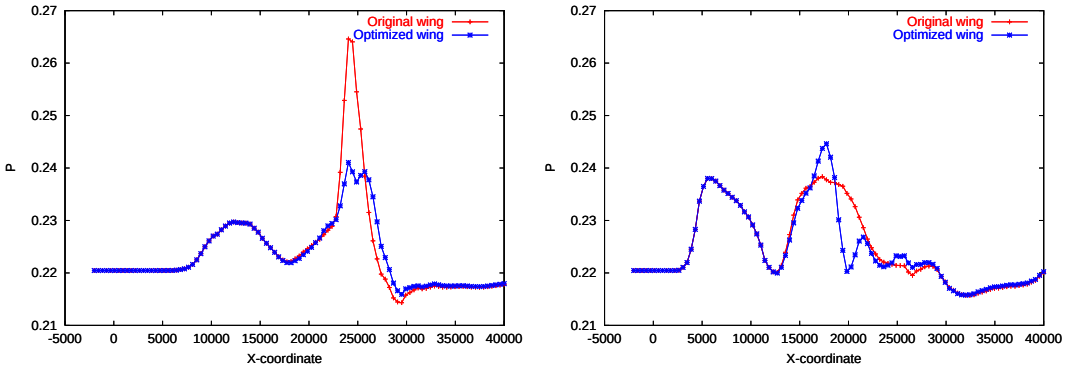

Figure 14: Supersonic Business Jet. Pressure along two lines below the wing, outside (left) and inside (right) the Mach cone.

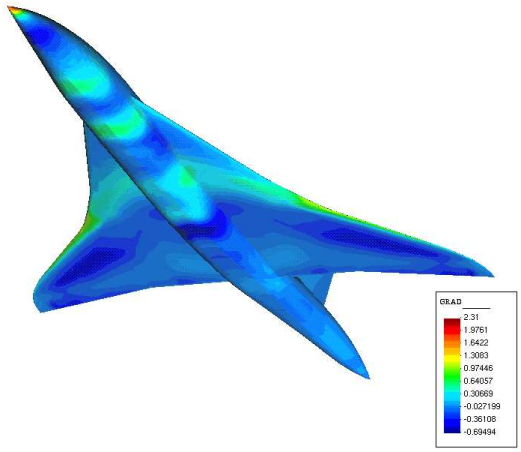

Figure 15: Supersonic Business Jet. Cost functional gradient distribution for the complete aircraft's surface.

5 Conclusion

We have proposed a new method for the optimization of aerodynamic supersonic shapes, which is based mainly on two original ideas. First, the extension of an additive multilevel method is applied to 3D shape parametrization. This approach is presented with a complete chain of arguments. We invoke a recent result on function smoothing of a multilevel preconditioners class. Using variational calculus, we have identified rather accurately the amount of smoothness that is required. Next a complete transposition to the discrete 3D context with unstructured tetrahedrization is built. This defines a tool that is applicable to real life optimal design problems. Finally we assess and confirm the soundness of these theoretical arguments with the aid of a concrete optimization problem.

In the practical applications, both the intermediate shapes we obtained are smoother and the convergence rates are better than those without preconditioning. This technique is also combined with several options well adapted to each other: CAD-free parametrization to work on the discretized shapes, Euler flow model with transpiration conditions which simulates the shape modifications produced by the optimization process, and a discrete adjoint approach, to deal with the eventually large dimension of the design variables space (up to 11000 surface grid points for a full Supersonic Business Jet optimization).

Laying on the optimum design side, the second original concept is the sonic boom optimization in itself. It is based on two pilars: *what* we in fact reduce and *how* we manage to reduce it. On one hand, we are not trying to reduce the sonic boom itself (i.e. the shock signature on the soil, in the far field), what requires additional (approximate) simulations falling out of the Euler flow equations scope. Instead of this, our goal is to reduce the pressure shock intensity in the near field below the plane, what we have called the sonic boom downwards emission, SBDE. On the other hand, we do it by modifying the aerodynamic shapes themselves. The parameters space is then the physical position of the skin mesh nodes, a mesh that in turn can be adapted to the needs of the flow field. Shape modifications are treated using a 3D transpiration condition. This particular kind of boundary condition is evaluated in this paper, resulting in a powerful and reliable tool for optimal shape design.

In combination with our simplified but effective manner for addressing the sonic boom emission, the shape optimization technique proposed in this paper allows to conduct the research among a very large family of shapes. Very simple examples show that bang-free geometries exist when no lift constraint is required, but a well known fact is that lift produces always sonic boom [4]

in supersonic flight condition. So when lifting bodies are seeked, shapes with flattened downwards halves play a particularly interesting role since in many cases they produce low sonic pressure rises, while keeping the lift. These kind of shapes are well reproduced by the proposed algorithm. We illustrate this point with a series of optimization examples with increasing shape complexity, rising up to a pre-industrial jet geometry. Additionally, the proposed scheme provides enough flexibility to tune the desired aerodynamic properties against the sonic boom downwards emission.

There are still several limitations in the accuracy of our results, that lead the way to future lines of research. The efficiency of the proposed approach can become an important issue when stiffer functional and constraints were considered and tenths of gradient iterations will be mandatory. Now, each iteration requires the complete solution of state and adjoint systems. In [24], we propose a new method inspired by Sequential Quadratic Programming (SQP) techniques for the simultaneous, or one-shot, solution of state, adjoint and optimality conditions. Concerning the cost functional model presented here, we believe that although it has shown a very efficient performance, it can be further improved.

In a following paper, we keep on developing the scheme here presented, by going deeper and farther. Deeper, because we work on new and more sophisticated versions of the cost functional. And farther because the next objective is to solve multiphysics problems by adding to the optimization cycle the aeroelastic coupling, all integrated in a Multi-Disciplinary Optimization (MDO) scheme. In this way, the sonic boom optimization will take into account also the deformations suffered by the aerodynamic shapes due to aeroelastic effects.

Acknowledgements : We thank Dassault Aviation for making available his Supersonic Business Jet's mesh for this project, and particularly Michel Mallet for reading and commenting this document, Gilbert Rogé et Michel Ravachol for stimulating discussions. We are also grateful to CINES (Centre Informatique National de l'Enseignement Supérieur) for providing the computational facilities where the largest examples were ran and to the French Ministry of Research for granting the project, under the coordination of Sébastien Candel and Denis Jeandel.

References

[1] F. Courty and A. Dervieux. Multilevel functional preconditioning for optimization. Technical Report, INRIA - Sophia Antipolis. 2002. To appear.

[2] M. Vázquez, B. Koobus, and A. Dervieux. Aerodynamical and sonic boom optimization of a supersonic aircraft. Technical Report RR-4520, INRIA - Sophia Antipolis. 2002.

[3] D.J. Maglieri and K.J. Plotkin. Aeroacoustics of Flight Vehicles: Theory And Practice. Acoustical Society of America, Publications. 1991.

[4] R. Seebas and B. Argrow. Sonic boom minimization revisited. AIAA Paper, 98-2956. 1998.

[5] J. Reuther and A. Jameson. Aerodynamic shape optimization of wing and wing-body configurations using control theory. AIAA Paper 95-0123. 1995.

[6] B. Mohammadi and O. Pironneau. Applied shape optimization for fluids. Clarendon Press - Oxford. 2001.

[7] A. Jameson. Aerodynamic design via control theory. Journal of Scientific Computing, 3:233–260. 1988.

[8] G. Kuruvila, S. Ta'asan, and M.D. Salas. Airfoil design and optimization by the one-shot method. AIAA Paper 95-0478, Jan. 1995

[9] H. Guillard and N. Marco. Some aspects of multigrid methods on non-structured meshes. In Proceedings of the Conference of Copper Mountain on Multigrid Methods, NASA, April 1995.

[10] F. Murat and J. Simon. Sur le contrôle par un domaine géométrique. Publication 76015, Laboratoire d'Analyse Numérique, Université Paris VI. 1976. (In French).

[11] F. Beux and A. Dervieux. Exact-gradient shape optimization of a 2D Euler flow. Finite Elements in Analysis and Design, 12:281–302. 1992.

[12] F. Beux. Conception optimale de formes aérodynamiques et méthodes d'approximations décentrées pour des écoulements incompressibles. PhD thesis, University of Nice, France. 1993. (In French).

[13] C. Farhat, K. Maute, B. Argrow, and M. Nikbay. A shape optimization methodology for reducing the sonic boom initial pressure rise. AIAA Paper, 2002-0145. 2002.

[14] S. Nadarajah, A. Jameson, and J. Alonso. An adjoint method for the calculation of remote sensitivities in supersonic flow. AIAA Paper, 2002-0261. 2002.

[15] J. Alonso, I. Kroo, and A. Jameson. Advanced algorithms for design and optimization of quiet supersonic platforms. AIAA Paper, 2002-0144. 2002.

[16] B. Mohammadi. Optimization of aerodynamic and acoustic performances of supersonic civil transports. In Center For Turbulence Research. Proceedings of the Summer Program 2002.

[17] H. Yamaguchi and Y. Nakamura. Optimization of low boom configuration of supersonic transports by genetic algorithm. AIAA Paper, 98-2899. 1998.

[18] W. P. Huffman, R. G. Melvin, D. P. Young, F. T. Johnson, J. E. Bussoletti, M. B. Bieterman, and C.L. Hilmes. Practical design and optimization in computational fluid dynamics. AIAA Paper 93-3111. 1993.

[19] G.D. Mortchelewicz. Résolution des équations d'Euler tridimensionnelles instationnaires en maillages non structurés. La Recherche Aérospatiale, (6):17–25, Novembre-Décembre 1991. (In French).

[20] N. Marco and A. Dervieux. Multilevel parametrization for aerodynamical optimization of 3D shapes. Finite Elements in Analysis and Design, Vol,26, 259-277. 1997.

[21] B. Koobus C. Farhat, C. Degand and M. Lesoinne. Torsional springs for two-dimensional dynamic unstructured fluid meshes. Comput. Meths. Appl. Mech. Engrg., 163:231–245. 1998.

[22] J. D. Anderson. Introduction To Flight. Mc. Graw - Hill. 2000.

[23] S.E. Cliff, J.J. Reuther, D.A. Saunders, and R.M. Hicks. Single-point and multipoint aerodynamic shape optimization of high-speed civil transport. Journal of Aircraft, 38(6):997–1005. 2001.

[24] A. Dervieux, F. Courty, M. Vázquez, and B. Koobus. Additive multilevel optimization and its application to sonic boom reduction. Numerical Methods for Scientific Computing - JP60 Meeting. Variational Problems and Applications. Jyvaskyla, Finland. 2002.